Computer Physics Communications 184 (2013) 270–283

Contents lists available at SciVerse ScienceDirect

Computer Physics Communications

journal homepage: www.elsevier.com/locate/cpc

The coupled 3D wave packet approach for triatomic reactive scattering in hyperspherical coordinates

Satrajit Adhikari [a,*], António J.C. Varandas [b]

[a] Department of Physical Chemistry, Indian Association for the Cultivation of Science, Jadavpur, Kolkata-700 032, India
[b] Departamento de Química, Universidade de Coimbra, 3004-535 Coimbra, Portugal

ARTICLE INFO

Article history:
Received 12 May 2012
Received in revised form
23 August 2012
Accepted 1 September 2012
Available online 5 September 2012

Keywords:
Triatomic reaction
Hypersherical coordinates
Reaction cross-section
Parallel computation

ABSTRACT

We have implemented the coupled three-dimensional wave packet approach in hyperspherical coordinates for time-dependent reactive scattering calculations of triatomic systems. The coupling of these wave packets arises through the rotation of the three particle plane by the Euler angles. The necessary transformation from Jacobi to hyperspherical coordinates for the initialization and the reverse transformation for the projection of the wave packet by the asymptotic state(s), and the coupled equation of motion are presented briefly. We demonstrate the workability and convergence profiles of the approach on the D + H_2 system for total angular momentum equal to zero and non-zero situations.

1. Introduction

The scattering experiments [1–8] that measure state-to-state integral and differential cross-sections of triatomic reactions demand rigorous, even full, quantum mechanical theory to interpret those results. There are significant progresses on the exact treatment of 3D as well as coupled 3D reactive scattering calculations on accurate potential energy surfaces (PESs) [9–11] for isotopic variants of H_3. Both time-independent and time-dependent approaches are employed for such calculations with zero and non-zero total angular momentum on a series of triatomic reactive systems.

At the end of the 1960's and beginning of the 1970's, a number of attempts had been made to solve quantum mechanically the simplest possible chemical reaction, the collision of an atom with a diatomic molecule on an electronically adiabatic (single-sheeted) PES, where the three atoms are confined to move on a space-fixed straight line (collinear) [12]. Baer and Kouri [13] developed an integral equation to tackle the non-collinear problem, where Saxon and Light [14] and Elkowitz and Wyatt [15] independently formulated their approximate close coupling equations to investigate the co-planar H + H_2 reaction. Wolken and Karplus [16] implemented the integro-differential equation derived by Miller [17] for 3D calculations on a H + H_2 system within the vibrational basis approximation. Kuppermann et al. [18] proposed an accurate method for solving the Schrödinger equation for the reaction A + BC → AB + C or AC + B on a single Born–Oppenheimer (BO) PES with the restriction that the motions of the three atoms are constrained on a space-fixed plane. An extensive theoretical advancement had been made on that approach by Kuppermann and Schatz [19].

The activity in quantum reactive scattering calculations for triatomic systems was renewed in a huge way during the mid 1980's. At that period of time, one can grossly identify four categories of theoretical approaches that were pursued for such calculations: The *R*-matrix propagation method developed by Light and co-workers [20]; the approaches based on hyperspherical coordinates to describe the system of atoms [21]; the *S*-matrix formulation of the Kohn variational principle by Miller and co-workers [17]; the work by Truhlar, Kouri and co-workers [22] who utilized a methodology based on the Newton variational principle employing a coupling scheme in the *T*-operator developed by Baer and Kouri [23].

With the advancement of more precise product detection methods [4,8], experiments have been carried out to measure rovibrationally state-to-state integral and differential cross-sections very accurately, and theoretical attempts made to interpret those results for various triatomic reactive systems [24–26]. During the 1990's, many calculations of state-to-state scattering cross-sections were performed by solving the time-independent nuclear Schrödinger equation by implementing the Coupled Channel (CC) approach in hyperspherical coordinates [27] such as to avoid the

* Corresponding author. Fax: +91 33 2473 2805.
E-mail addresses: pcsa@iacs.res.in (S. Adhikari), varandas@qtvs1.qui.uc.pt (A.J.C. Varandas).

0010-4655/$ – see front matter © 2012 Elsevier B.V. All rights reserved.
doi:10.1016/j.cpc.2012.09.001

coordinate transformation from reactant to product channels. The hyperspherical coordinates solve this problem by smoothly changing the frame of reference from the reactant, A+BC, to the products, AC + B and AB + C. The CC method in hyperspherical coordinates has yielded very accurate state-to-state cross-sections and reaction probabilities for a variety of triatomic reactions. However, the computational time for the CC approach scales inefficiently with increasing J (total angular momentum) and N_i (the number of basis functions used for the ith internal coordinate), and generally, such cost scales as $(J\prod N_i)^3$.

Time-dependent approaches based on wave packets were introduced into reactive scattering [28], where such methods overcome the computational scaling as $J\prod_i N_i \sum_i \log N_i$ (if ith degree of freedom is represented on an equally spaced grid basis), and are ideal for *multi-core multi-node* computers to parallelize while solving all partial waves [29] of the time-dependent Schrödinger equation (TDSE). There are many good reasons for pursuing the time-dependent wave packet methods: (a) A large energy range in the translational coordinate can be covered by a single wave packet; (b) The blending of classical and quantum mechanics to develop new methodologies becomes possible; (c) If grid methods are used, the dissociation events are automatically accounted even at the important high energy region; (d) As the system mass and/or energy increases, the CPU requirement of grid methods will not necessarily increase as state expansion approaches; (e) It may be easy to extend such time-dependent grid methods to non-adiabatic events, where multiple electronic PESs are coupled with each other. As long as the calculation of the Fourier transform of the wave function is the most time consuming step, the CPU time should increase only about linearly with the number of sheets in the PES, hence the computation time should remain approximately constant via appropriate parallelization of the equation of motion for the different sheets.

Although there were time-dependent wave packet calculations based on the methodology formulated in Jacobi coordinates for initial state resolved total cross-sections [30] and total reaction probability [31], most such calculations were only for the simplest case, $J = 0$, or could not be compared for non-zero angular momentum cases with the corresponding time-independent results because of the inherent reactant-product coordinate transformation problem. Indeed, there were few attempts to transform the coordinates when the wave packet reaches the strong interaction region [32], but such approaches appear either to be expensive or inaccurate. Conversely, when Zhang and co-workers [33] introduced the "reactant-product decoupling" (RPD) equation, such an approach has been recasted by Kouri and co-workers [34], Zhang and co-workers [35], and Althorpe [36] over a period of time to achieve an efficient algorithm. The calculations based on RPD algorithms for initial state resolved integral and differential cross-sections appear accurate and fully converged even for non-zero total angular momenta. On the other hand, Gray and Balint-Kurti [37] developed an accurate time-dependent quantum dynamics method with real wave packets for reactive scattering, which has been implemented to calculate integral and differential cross-sections of various reactive systems.

The time-dependent wave packet approach using hyperspherical coordinates is convenient for treating reactive processes due to the equivalent description of all rearrangement channels. Since the problem of any triatomic reaction is a 4D quantum mechanical one, it is possible to formulate the "exact" solution in terms of coupled 3D wave packets. Each 3D wave packet represents the hyperradius, ρ, and hyperangles, θ and ϕ, where such partial waves arise due the quantization of rotation of the three particle plane. Billing and co-workers [38] formulated the time-dependent wave packet approach using hypersperical coordinates, and performed 3D as well as coupled 3D wave packet calculations on the D + H_2 system for the simplest case, $J = 0$ and $J = 1$, respectively. At present, we implement the same formulation to carry time-dependent wave packet calculation on triatomic system for $J = 0$ and $J \neq 0$ cases. Although there has been some progress on the methodological development and calculations in Jacobi coordinates involving two electronic states [39,40], we believe there is enough scope to formulate new approaches and carry out calculations in hypershperical coordinate system because of its inherent advantages. A major aim for implementing this time-dependent wave packet approach in hyperspherical coordinates is to extend such a methodology beyond Born–Oppenheimer, *i.e.*, to multi-surface reactive scattering.

2. Theory

2.1. Initial wave packet in hyperspherical coordinates

The channel (reactive/non-reactive) independent asymptotic solution to the reactive scattering of a triatomic system in Jacobi coordinates could be of the following form:

$$\Psi \rightarrow \frac{1}{Rr}\sum_{\gamma' vjl} u^{Jl'}_{\gamma\gamma'}(R) y^{JM}_{jl}(\hat{R},\hat{r})\phi_{vj}(r), \tag{1}$$

where y^{JM}_{jl} and ϕ_{vj} are Arthurs–Dalgarno (AD) states [41] and vibrational wave packets, respectively. The vibrational wave packet, ϕ_{vj}, depends upon the rotational quantum number j through the centrifugal coupling term. The volume element is given by:

$$R^2 dR\, r^2 dr d\hat{R} d\hat{r}, \tag{2}$$

where

$$d\hat{R}\, d\hat{r} = \sin\Theta'\, d\Theta'\, d\Phi' \sin\eta\, d\eta\, d\xi. \tag{3}$$

The distance from the atom (A) to the center of mass of the diatomic molecule (BC) is R and the orientation of R in a space-fixed coordinate system is given by the angles Θ' and Φ' (see Fig. 1). The bond distance of the BC molecule is r and its orientation in a body-fixed coordinate system (with R' axis along z) is given by the angles η and ξ. It is obvious that the function $(1/R)u^{Jl}_{\gamma\gamma'}(R)$ is normalized on $R^2\, dR$, $(1/r)\phi_{vj}(r)$ on $r^2\, dr$ and the AD states $y^{Jl}_{jl}(\hat{R}\,\hat{r})$ on $d\hat{R}\, d\hat{r}$.

In Jacobi coordinates, the wave packet can be initialized as:

$$\Psi \rightarrow \frac{1}{r}\phi_{vj}(r) y^{JM}_{jl}\frac{1}{R}\chi(R), \tag{4}$$

where $\frac{1}{R}\chi(R)$ is a wave packet normalized on $R^2\, dR$.

In hyperspherical coordinates [42], the corresponding volume element is

$$\frac{1}{8}\rho^5 \sin\theta\cos\theta\, d\theta\, d\phi\, d\alpha \sin\beta\, d\beta\, d\gamma, \tag{5}$$

where ρ is the hyperradius, and θ and ϕ are the two hyperangles. These three variables define the geometry of the ABC plane, while the orientation of this plane in space is defined by the three Euler angles α, β and γ.

The wave function used in our approach is given by the following transformation:

$$\begin{aligned}\psi &= (1/\sqrt{8})\rho^{5/2}\sqrt{\sin\theta\cos\theta}\,\Psi \\ &= (1/\sqrt{8})\rho^{5/2}\sqrt{\sin\theta\cos\theta}\frac{1}{r}\phi_{vj}(r) y^{JM}_{jl}\frac{1}{R}\chi(R),\end{aligned} \tag{6}$$

where ψ has the volume element:

$$d\rho\, d\theta\, d\phi\, d\alpha \sin\beta\, d\beta\, d\gamma. \tag{7}$$

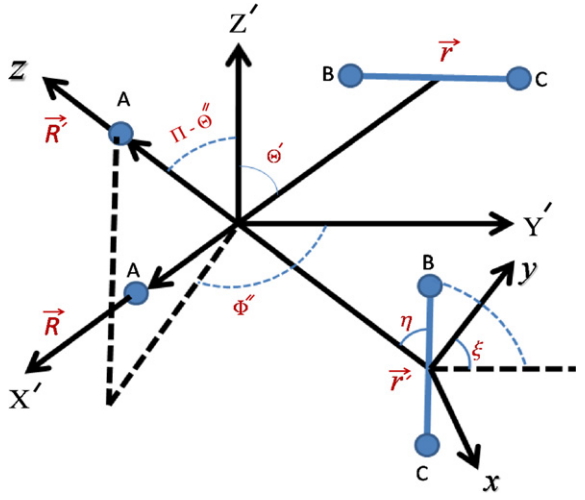

Fig. 1. The position of the three atoms in the space-fixed coordinate system (X', Y', Z') and the body-fixed coordinate system (x, y, z).

Substituting the Jacobi variables in terms of hyperspherical coordinates for the reactant channel (A + BC) (see Appendix A),

$$Rr = \frac{1}{2}\rho^2\sqrt{1-\sin^2\theta\cos^2\phi}, \tag{8}$$

and the initial wavefunction in Eq. (6) yields:

$$\psi = \frac{1}{\sqrt{8}}\rho^{5/2}\sqrt{\sin\theta\cos\theta}\,\frac{2}{\rho^2\sqrt{1-\sin^2\theta\cos^2\phi}}\phi_{vj}(r)y_{jl}^{JM}\chi(R)$$

$$= \sqrt{\frac{\rho}{2}\left(\frac{\sin\theta\cos\theta}{1-\sin^2\theta\cos^2\phi}\right)}\phi_{vj}(r)y_{jl}^{JM}\chi(R), \tag{9}$$

where the orientation angle of the diatom and the Jacobian are defined as:

$$\sin\eta = \frac{\cos\theta}{\sqrt{1-\sin^2\theta\cos^2\phi}} \tag{10}$$

and

$$J(Rr\eta|\rho\theta\phi) = \frac{\rho}{2}\frac{\sin\theta}{\sqrt{1-\sin^2\theta\cos^2\phi}}, \tag{11}$$

respectively.

The initial wavefunction can therefore be written as:

$$\psi = \sqrt{\sin\eta\,J(Rr\eta|\rho\theta\phi)}\;\phi_{vj}(r)y_{jl}^{JM}\chi(R). \tag{12}$$

On the other hand, the wave packet ψ in Eq. (12) can be expanded in terms of the Wigner **D** matrix as:

$$\psi = \sum_{K=-J}^{J}\Phi_K(\rho,\theta,\phi)\sqrt{\frac{2J+1}{8\pi^2}}D_{MK}^{J*}(\alpha,\beta,\gamma), \tag{13}$$

where $\sqrt{\frac{2J+1}{8\pi^2}}D_{MK}^{J}$ is normalized on $d\alpha\ \sin\beta\,d\beta\,d\gamma$. Thus, we have

$$\sum_K\int d\rho\,d\theta\,d\phi\,|\Phi_K|^2 = 1 \tag{14}$$

where the summation implicitly considers all allowed K values.

Equating Eq. (13) with Eq. (12), the functional form of the initial wave packet for the K th component $\Phi_K(\rho,\theta,\phi)$ is given by:

$$\Phi_K(\rho,\theta,\phi) = \sqrt{\frac{2J+1}{8\pi^2}}\int d\alpha\int d\beta\ \sin\beta \times\int d\gamma\ D_{MK}^{J}(\alpha\beta\gamma) \times\sqrt{\sin\eta\,J(Rr\eta|\rho\theta\phi)}\;\phi_{vj}(r)y_{jl}^{JM}\chi(R). \tag{15}$$

This can be written in a more compact form by employing the AD states y_{jl}^{JM} in terms of **D** matrix and spherical harmonics (Y), namely

$$y_{jl}^{JM} = (-1)^{j-l-M}\sqrt{(2J+1)(2l+1)/4\pi} \times\sum_\mu\begin{pmatrix} j & l & J\\ \mu & 0 & \mu\end{pmatrix}Y_{j\mu}(\eta,\xi)D_{-M,-\mu}^{J}(\Phi',\Theta',0), \tag{16}$$

where $3-j$ symbols are the linear combining coefficients. Thus, by substituting

$$Y_{j\mu}(\eta,\xi) = C_{j\mu}(\eta)\exp(i\mu\xi), \tag{17}$$

and

$$D_{M,-\mu}^{J}(\Phi',\Theta',\xi) = \exp(-iM\Phi')d_{M,\mu}^{J}(\Theta')\exp(i\mu\xi), \tag{18}$$

Eq. (16) assumes the form:

$$y_{jl}^{JM} = \sqrt{(2J+1)(2l+1)/4\pi}\ (-1)^{j-l-M} \times\sum_\mu\begin{pmatrix} j & l & J\\ \mu & 0 & -\mu\end{pmatrix}C_{j\mu}(\eta)D_{-M,-\mu}^{J}(\Phi',\Theta',\xi). \tag{19}$$

Without loss of generality, it is possible to set the projection quantum number M equal to zero and thereby,

$$D_{0,-\mu}^{J}(\Phi',\Theta',\xi) = \exp(i\mu\xi)d_{\mu0}^{J}(\Theta') = \sqrt{\frac{4\pi}{2J+1}}\,C_{J\mu}(\Theta')\exp(i\mu\xi) \tag{20}$$

and

$$D_{0,K}^{J}(\alpha,\beta,\gamma) = \exp(-iK\gamma)(-1)^K\sqrt{\frac{4\pi}{2J+1}}C_{JK}(\beta). \tag{21}$$

If Eq. (20) is now substituted in Eq. (19), the AD functions, y_{jl}^{JM}, assume the form:

$$y_{jl}^{JM} = \sqrt{(2l+1)}\ (-1)^{j-l-M} \times\sum_\mu\begin{pmatrix} j & l & J\\ \mu & 0 & -\mu\end{pmatrix}C_{j\mu}(\eta)C_{J\mu}(\Theta')\exp(i\mu\xi). \tag{22}$$

By inserting next Eqs. (21) and (22) into Eq. (15), the final form of the wave packet in hyperspherical coordinates becomes:

$$\Phi_K = \sqrt{2\pi\ \sin\eta\,J(Rr\eta|\rho\theta\phi)(2l+1)}\phi_{vj}(r)\ \chi(R)(-1)^{j-l} \times\sum_\mu\begin{pmatrix} j & l & J\\ \mu & 0 & -\mu\end{pmatrix}C_{j\mu}(\eta)A_{K\mu}, \tag{23}$$

where

$$A_{K\mu} = (-1)^K\int_0^{2\pi}d\gamma\int_0^{\pi}d\beta\ \sin\beta \times\exp(-iK\gamma+i\mu\xi)C_{JK}(\beta)C_{J\mu}(\Theta'), \tag{24}$$

with the orthonormality condition:

$$\sum_K A_{K\mu}^{*}A_{K\mu'} = \delta_{\mu\mu'}\quad\text{(See Appendix B)}. \tag{25}$$

While constructing the **A** matrix, the following relationship (Appendix A) between the orientation (Θ' and ξ) and Euler (β and γ) angles is employed:

$$\cos\Theta' = -\sin\beta\ \cos\gamma, \tag{26}$$

$$\sin\xi = \cos\beta/\sin\Theta'. \tag{27}$$

The part of the wave function corresponding to A − BC relative motion (translation) is described by a Gaussian wave packet,

$$\chi(R) = N \exp[-ik_0 R - a(R - R_0)^2], \tag{28}$$

where

$$a = 1/(4\sigma^2 - iq), \tag{29}$$

$$q = 2(R_0 - R_f)/k_0, \tag{30}$$

$$N = (A/\pi)^{1/4}, \tag{31}$$

$$A = 8\sigma^2/(16\sigma^4 + q^2). \tag{32}$$

The center of the wave packet is initially at $R = R_0$ and will, in the absence of forces, move in the negative R direction with momentum $p_0 = \hbar\, k_0$. The imaginary term in the denominator of the constant a will keep the wave packet narrow until it reaches the "focal point", R_f. The initial collisional energy determines the wavevector (k_0) by employing the triatomic center of mass for the reactants, $\mu_R = m_A(m_B+m_C)/(m_A+m_B+m_C)$, where the diatomic (BC) reduced mass is given by $\mu_r = m_B m_C/(m_B + m_C)$.

2.2. The Hamiltonian and the coupled equations

The Hamiltonian operator describing a three-particle system expressed in terms of Johnson's hypersherical coordinates [42] assumes the form:

$$\begin{aligned}\hat{H} = &-\frac{\hbar^2}{2\mu_R}\frac{\partial^2}{\partial\rho^2} + \frac{2}{\mu_R\rho^2}\hat{L}^2(\theta,\phi)\\ &+ \frac{1}{\mu_R\rho^2}\left[\frac{\hat{J}_x^2}{1-\sin\theta} + \frac{\hat{J}_y^2}{1+\sin\theta} + \frac{\hat{J}_z^2}{2\sin^2\theta}\right]\\ &- \frac{2\cos\theta\,\hat{J}_z\hat{P}_\phi}{\mu_R\rho^2\sin^2\theta} + V(\rho,\theta,\phi) + \Delta V(\rho,\theta),\end{aligned} \tag{33}$$

where

$$\hat{J}_z = -i\hbar\left(\frac{\partial}{\partial\gamma}\right), \tag{34}$$

$$\hat{P}_\phi = -i\hbar\left(\frac{\partial}{\partial\phi}\right), \tag{35}$$

$$\hat{L}^2(\theta,\phi) = -\hbar^2\left[\frac{\partial^2}{\partial\theta^2} + \frac{1}{\sin^2\theta}\frac{\partial^2}{\partial\phi^2}\right], \tag{36}$$

$$\Delta V(\rho,\theta) = -\frac{\hbar^2}{2\mu_R\rho^2}\left[\frac{1}{4} + \frac{4}{\sin^2 2\theta}\right]. \tag{37}$$

Although the angular momentum operators $\hat{J}_x$ and $\hat{J}_y$ are functions of the Euler angles α, β and γ, their forms are not needed because the Hamiltonian (Eq. (33)) can be simplified using the following relation:

$$\hat{J}^2 = \hat{J}_x^2 + \hat{J}_y^2 + \hat{J}_z^2, \tag{38}$$

leading to:

$$\begin{aligned}\hat{H} = &-\frac{\hbar^2}{2\mu_R}\frac{\partial^2}{\partial\rho^2}\\ &+ \frac{2}{\mu_R\rho^2}\hat{L}^2(\theta,\phi) + \frac{\hat{J}^2 - \hat{J}_z^2}{\mu_R\rho^2\cos^2\theta} + \frac{\hat{J}_z^2 - 4\cos\theta\,\hat{J}_z\hat{P}_\phi}{2\mu_R\rho^2\sin^2\theta}\\ &+ \frac{\sin\theta}{\mu_R\rho^2\cos^2\theta}\frac{1}{2}[\hat{J}_+^2 + \hat{J}_-^2] + V(\rho,\theta,\phi) + \Delta V(\rho,\theta),\end{aligned} \tag{39}$$

where the raising and lowering operators have been introduced using the relation:

$$\hat{J}_x^2 - \hat{J}_y^2 = \frac{1}{2}[\hat{J}_+^2 + \hat{J}_-^2]. \tag{40}$$

When we substitute the wave packet ψ (Eq. (13)) and the Hamiltonian (Eq. (39)) into the time-dependent Schrödinger equation (TDSE), the following set of coupled equations are obtained in terms of partial waves (Φ_K):

$$\begin{aligned}i\hbar\frac{\partial\Phi_K}{\partial t} = &\left\{-\frac{\hbar^2}{2\mu_R}\frac{\partial^2}{\partial\rho^2} + \frac{2}{\mu_R\rho^2}\hat{L}^2(\theta,\phi)\right.\\ &+ \frac{\hbar K(\hbar K - 4\cos\theta\,\hat{P}_\phi)}{2\mu_R\rho^2\,\sin^2\theta}\\ &+ \frac{\hbar^2[J(J+1) - K^2]}{\mu_R\rho^2\cos^2\theta}\\ &\left.+ V(\rho,\theta,\phi) + \Delta V(\rho,\theta)\right\}\Phi_K\\ &+ \frac{\sin\theta}{\mu_R\rho^2\cos^2\theta}[M_{K,K+2}\Phi_{K+2} + M_{K,K-2}\Phi_{K-2}],\end{aligned} \tag{41}$$

where the last term couples the component Φ_K to $\Phi_{K\pm2}$ via the coupling element $M_{K,K\pm2}$

$$M_{K,K\pm2} = \frac{\hbar^2}{2}\sqrt{(J\mp K)(J\pm K+1)(J\mp K-1)(J\pm K+2)}. \tag{42}$$

A discrete representation of the partial waves $\Phi_K(\rho,\theta,\phi)$ on three-dimensional grids are introduced to propagate the coupled wave packets with time.

2.3. Analysis of the outgoing wave packet

It is possible to project the outgoing wave packet onto asymptotic eigenstates at a fixed value of the hyperradius ρ. Since, in hypersherical coordinates, all distances are represented by this single variable, the inelastic coupling between different vibrational states will vanish very slowly with ρ. An asymptotic propagation to large values of the hyperradius is therefore necessary before accurate reaction probabilities could be calculated. In the present work, we project the wave packet onto asymptotic eigenstates at a fixed value of R which greatly simplifies or entirely removes the asymptotic propagation part of the problem [38].

The scattering amplitude in the channel specified by vibrational, rotational and orbital quantum numbers v', j', l' is obtained as:

$$\begin{aligned}u^J_{v'j'l'}(R;t) = &\,4R\int dr\\ &\times\int d\eta\, r\sin\eta\,\rho^{-5/2}(\sin 2\theta)^{-1/2}\phi_{v'j'}(r)\\ &\times\sum_{K\mu'} g_{j'l'\mu'}A^*_{K\mu'}C_{j'\mu'}(\eta)\Phi_K(\rho,\theta,\phi),\end{aligned} \tag{43}$$

where

$$g_{jl\mu} = \sqrt{2\pi(2l+1)}(-1)^{j-l}\begin{pmatrix} j & l & J\\ \mu & 0 & -\mu\end{pmatrix}. \tag{44}$$

The integration is performed over the (θ,ϕ) grid using the relations:

$$\rho = \sqrt{2}d_i\, R/\sqrt{1 - \sin\theta\cos(\phi - \epsilon_i)}, \tag{45}$$

$$r = \frac{d_i\,\rho}{\sqrt{2}}\sqrt{1 + \sin\theta\cos(\phi - \epsilon_i)}, \tag{46}$$

$$\sin\eta = \cos\theta/\sqrt{1 - \sin^2\theta\cos^2(\phi - \epsilon_i)}, \tag{47}$$

with the Jacobi factor (for fixed R) given by:

$$J(r,\eta|\theta,\phi) = \frac{d_i^2 R\sin\theta}{[1-\sin\theta\cos(\phi-\epsilon_i)]\sqrt{1-\sin^2\theta\cos^2(\phi-\epsilon_i)}}, \quad (48)$$

where d_i and ϵ_i are channel dependent constants. Since the projection is performed for a fixed value of R and the hyperradius is a function of R, θ and ϕ, it is necessary to interpolate on the grid in order to find the corresponding value of Φ_K.

When the wave packet has passed the projection region the amplitudes are Fourier transformed from time to energy space:

$$b^J_{v'j'l'}(E;R) = \frac{1}{\sqrt{2\pi}}\int dt\; u^J_{v'j'l'}(R;t)\exp(iEt/\hbar). \quad (49)$$

These amplitudes are now expanded on incoming and outgoing waves,

$$b^J_{v'j'l'} = A^{\rm in}_{v'j'l'}k_{v'j'}R\,h^-(k_{v'j'}R) + A^{\rm out}_{v'j'l'}k_{v'j'}R\,h^+(k_{v'j'}R), \quad (50)$$

where

$$h^{\pm}(k_{v'j'}R) = -n_l(k_{v'j'}R) \pm ij_l(k_{v'j'}R) \quad (51)$$

and j_l and n_l are spherical Bessel and Neumann functions, respectively. The projection on the incoming component of the scattered wave packet should, of course, be zero. The reaction probability from the initial state (vjl) to the product state $(v'j'l')$ is obtained as the ratio of the outgoing and incoming fluxes,

$$P_{v'j'l'\leftarrow vjl} = \frac{F_{v'j'l'}}{F_{vjl}}, \quad (52)$$

where

$$F_{v'j'l'} = \frac{1}{\mu_{\rm out}}k_{v'j'}|A^{\rm out}_{v'j'l'}|^2, \quad (53)$$

$$F_{vjl} = \frac{1}{\mu_{\rm in}}k_{vj}|c^l_E|^2, \quad (54)$$

c^l_E is the component with energy E contained in the initial wave packet, k_{vj} the wave number of the initial channel vj, and $\mu_{\rm in}$ and $\mu_{\rm out}$ the appropriate center of masses for the reactants and products, respectively. The weight in energy space is related (see Appendix D) to the weight in k space through the relation:

$$|c^l_E|^2 = \left(\frac{\mu_{\rm in}}{\hbar k}\right)^2|c^l_k|^2. \quad (55)$$

$|c^l_k|^2$ can be obtained analytically for a Gaussian wave packet as:

$$|c^l_k|^2 = \sqrt{2/\pi}\;\sigma\;\exp[-2\sigma^2(k-k_0)^2], \quad (56)$$

but this expression is only valid for a free particle, i.e., corresponding to a system initialized at very large separation. On the other hand, if the incoming or outgoing wave packet is initialized or analyzed at a moderate value of R, the effective potential at the same R appears as $[V(R)+l(l+1)/2\mu R^2]$, where the potential is averaged over the spherical DOFs (degree of freedom), θ and ϕ, to calculate the effective potential $V(R)$.

2.4. The absorbing potential

The outgoing wave packet must be removed from the grid just after the projection but before it reaches the grid boundary at $\rho_{\rm max}$. This is accomplished by adding a negative imaginary potential to the last grid points for the hyperradius. This absorbing potential has no physical meaning, it is located far away from the interaction region but is a device used to avoid reflection. The form of the imaginary potential is arbitrary, the only requirement is that the scattering amplitudes should be independent of the type of function used. In the present work, we use an absorbing potential of the following form:

$$V_{\rm lm}(\rho) = -\frac{iV^{\rm max}_{\rm lm}}{\cosh^2[(\rho_{\rm max}-\rho)/\alpha]}, \quad \rho\geq\rho_{\rm lm}, \quad (57)$$

where $\rho_{\rm lm}$ is the starting point for the absorbing potential. The performance of the imaginary potential is not very sensitive to the choice of $V^{\rm max}_{\rm lm}$, but with α. The error at low energies indicates that these components are not absorbed efficiently. To improve the absorption, the magnitude of the absorbing potential should be decreased. This will, however, lead to reflection at higher energies. We therefore decided to decrease α linearly with time during the absorption of the wave packet. By doing so the slow moving energy components will experience an absorbing potential of a magnitude small enough to avoid reflection. This procedure led to a very uniform error distribution over the entire energy range.

3. Propagation and computation details

We propagate the wave packet(s) in time by employing the iterative Lanczos reduction technique. Such an algorithm is known as a short time propagator, capable of automatically controlling recursion by monitoring the magnitude of the last few vectors, and accurate enough for the analysis of the outgoing wave packet. In order to recover the wave packet after each propagation step, we need to store the transformation matrix constituted with Lanczos recursion vectors. Since it is possible to store this matrix in the core memory, one can avoid repeated calculation for half of such vectors are required for the next time step.

Although the actual bottleneck is the evaluation of the kinetic energy operator by using the Fast Fourier Transformation (FFT) method, it has the favorable property that the computational effort scales as $cN\log N$, where N is the total number of grid points on the ρ, θ and ϕ coordinates. However, the CPU time is still very high for the recursive calculation of the kinetic energy operators for iterative Lanczos propagation on a number of grid points up to 2×10^6 ($256\times64\times128$). In particular, because the domain of θ varies from 0 to $\pi/2$ in the hyperspherical coordinate system, the grid size needs to be doubled in that coordinate so that the basis functions (plane waves) vanish at $\theta=0$ and π leading to a sine transformation (see Appendix C). Moreover, the computational cost increases tremendously as the total angular momentum J increases, particularly because the projection of the time dependent wave packets on asymptotic states (v',j') arising due to various orbital angular momentum (l').

Indeed, one can reduce the huge computational cost through parallelization. The computation for a set of partial waves (Ks) is then carried out in different nodes by employing the *MPI* thread, where the time propagation and its projection for each partial wave are performed through *OpenMp* parallelization in a particular node. Fig. 2 displays the computational cost as a function of J for the serial and parallel algorithms. The results speak for themselves by showing that the labor with parallelization is done much faster than with a serial implementation.

4. Results and discussions

For the testing purposes and the sake of comparisons with previous work, we perform 3D wave packet $[\Phi(\rho,\theta,\phi)]$ dynamics on the D + H_2 ($v=0,1; j=0$) system using the Siegbahn–Liu–Truhlar–Horowitz (SLTH) [9] as well as Double Many - Body

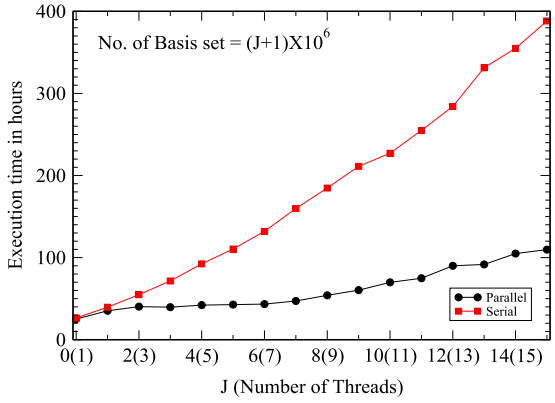

Fig. 2. The computation time (hours) as a function of J for various number of basis sets. The red square and black circle symbols depict the computation time (hour) for serial and parallel (OpenMp) runs, respectively.

- Expansion (DMBE) [11] BO PESs to calculate non-reactive [D + H_2 (v', j')] and reactive [DH(v', j')+H] transition probabilities over a range of initial kinetic energies of the incoming atom (D) with total angular momentum $J = 0$. Moreover, for the D + H_2 $(v = 0, j = 0)$ system, coupled 3D wave packet [$\Phi_K(\rho, \theta, \phi)$] dynamics has been carried out on the same BO PESs for a series of non-zero total angular momenta, $J = 1$–20, where the wave packet of the system is constituted with J or $J + 1$ number of partial waves depending upon the initial rotational state (j) of the diatom. Table 1 depicts the various parameters involved in our dynamical calculations.

The modulus of the time-dependent wave packet can be conveniently visualized in hyperspherical coordinates due to its high symmetry, where the densities are mapped onto the equator of a hypersphere with radius ρ and hyperangles θ and ϕ. In Figs. 3–5, we have used a stereographic projection technique [43] with $\beta = \sin\theta\cos\phi$ and $\gamma = \sin\theta\sin\phi$ to display the time-dependent density for $J = 0$, 10 and 20 cases, respectively, where the collisional energy of the incoming atom D is 1.11 eV and the initial state of the diatom H_2 is $v = 0, j = 0$. The plots clearly illustrate the change of reactive transition probabilities to non-reactive ones with increasing total angular momentum J at a fixed total energy of 1.34 eV.

Figs. 6 and 7 display vibrationally resolved reaction probabilities due to the collision of D + H_2 system with initial state $(v = 0, j = 0)$ and $(v = 1, j = 0)$, respectively, for total angular momentum $J = 0$, where in all cases, we compare our calculated probabilities with those obtained by Zhang and Miller [17] employing the time-independent Kohn variational principle based *S-matrix* approach. When calculations are performed on SLTH PES, Fig. 6a demonstrates the convergence of the probabilities with respect to the increasing number of grid points on different coordinates (ρ, θ, ϕ). Although the reaction probabilities are fully converged with the set of grid points, $128 \otimes 64 \otimes 128$ for the ρ, θ and ϕ coordinates, we prefer to perform our calculations with the set

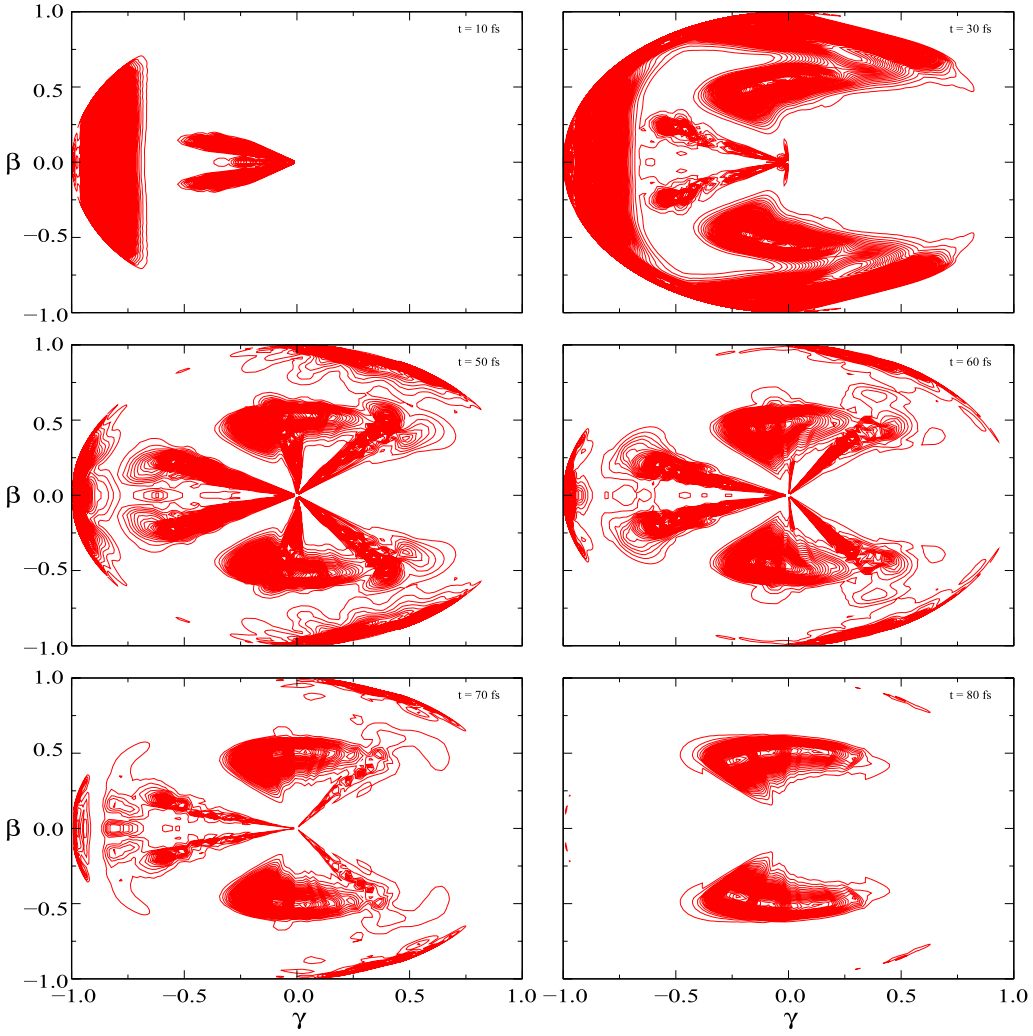

Fig. 3. Time-dependent density of the wave packet ($|\psi^2|$) for $J = 0$. The axes β and γ are defined by $\sin\theta\cos\phi$ and $\sin\theta\sin\phi$, respectively.

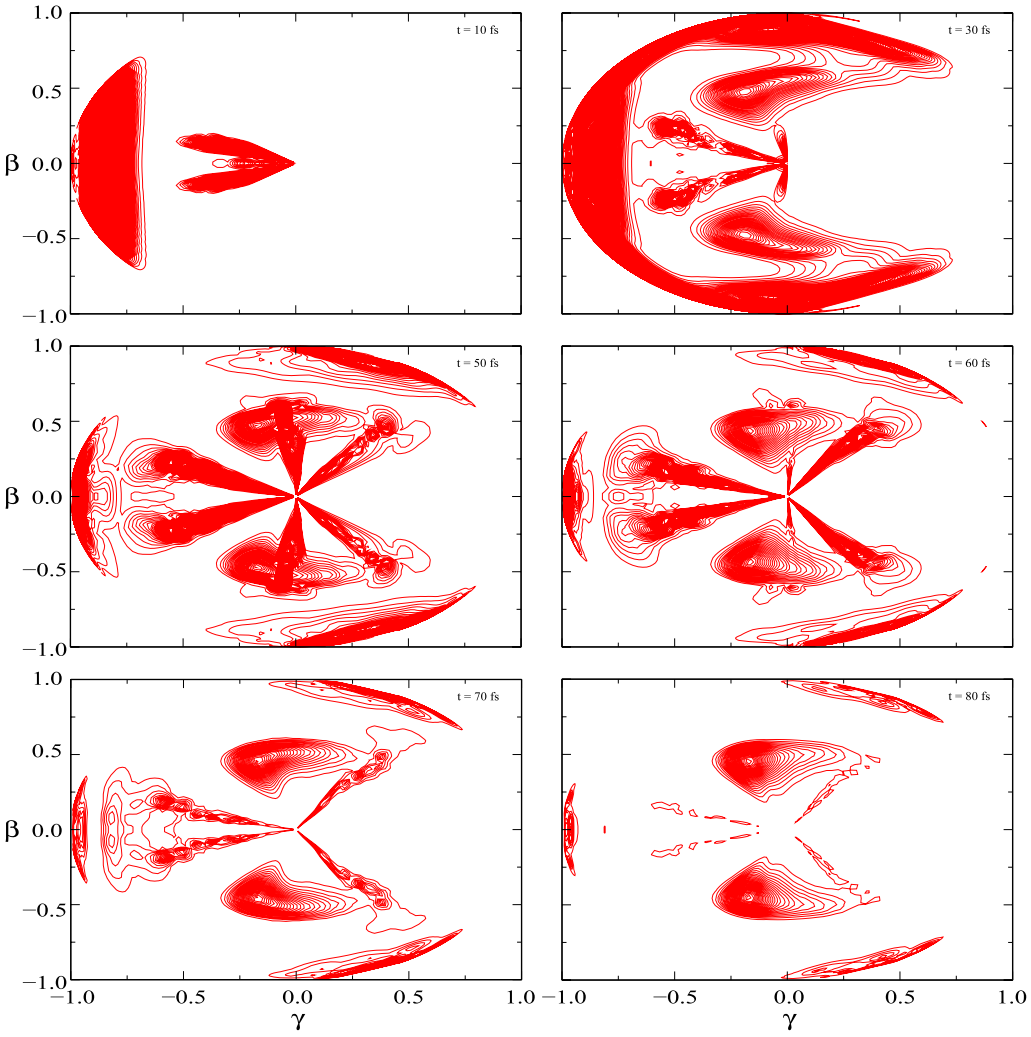

Fig. 4. Same as Fig. 3 for $J = 10$.

256 ⊗ 64 ⊗ 128. Indeed, because the projection on a particular R (i.e., R^*) requires interpolation of the wave packet on the ρ coordinate, we perform dynamics calculations with a high number of grid points (256) in that coordinate. On the other hand, Fig. 6b depicts the comparison of the reaction probabilities obtained by using SLTH and DMBE PESs, where transition probabilities from DMBE PES are slightly closer with Zhang and Miller's [17] results than the SLTH ones. When we carry out the dynamics on DMBE potential and analyze at different asymptotic projection distance (R^*), Fig. 6c displays those probabilities which appear fully converged after 3 Å onwards over a long range of initial KE of the incoming atom (D). In summary, Fig. 6 shows that the agreement between our calculated results either by using SLTH or DMBE PESs and the ones of Zhang and Miller is reasonable over the entire energy range, whereas in Fig. 7, we find that there is some disagreement at all energies, particularly, those obtained from SLTH PES and the transition probabilities for $v' = 1$ with DMBE PES. In general, it appears reaction probabilities from DMBE PES lie somewhat closer to Zhang and Miller [17] results carried out on SLTH. Although the threshold behavior of our calculated probability is quite correct, the resonances are slightly different and that may be due to time-independent versus time-dependent approach or to some remote extent to the adiabatic BO PES itself.

Fig. 8 depicts the rovibrational reaction probabilities calculated by using SLTH and DMBE PESs for the collision D + H_2 ($v = 0$, $j = 0$) with total angular momentum $J = 0$ as a function of rotational quantum number, j', for the product DH (v', j') at different initial kinetic energies of the incoming atom, D. At the energies of 1.0 and 1.5 eV, the agreement between the two calculated results for $v' = 0$ with Zhang and Miller [17] is quite encouraging, whereas the probabilities calculated for $v' = 0$ and 1 at initial kinetic energies of 0.6 and 1.0 eV show some disagreement, particularly, at high j' values. The other reason for some disagreement could be the projection of the wave packet on various initial kinetic energies starting with a specific total energy of the system.

In Fig. 9, we present the reaction probabilities calculated by employing SLTH and DMBE PESs for the collision, D + H_2 ($v = 0, j = 0$) as a function of the initial kinetic energy of the incoming atom, D, when the total angular momentum (J) of the system is 1. In the same plot, the corresponding data from Miller and Zhang on SLTH are also depicted. The reaction probabilities obtained by using SLTH PES for $v' = 0$ and 2 agree quite closely with the ones of Zhang and Miller over the entire energy range, but there are some differences at higher energies for the reaction probabilities on $v' = 1$. On the other hand, the transition probabilities calculated with DMBE PES have good agreement with Zhang and Miller [17] over the entire energy range for all final vibrational states (v'). Finally, in Figs. 10 and 11, we demonstrate the reaction probability obtained by using SLTH and DMBE PESs for $v' = 0$ and 1, respectively, as a

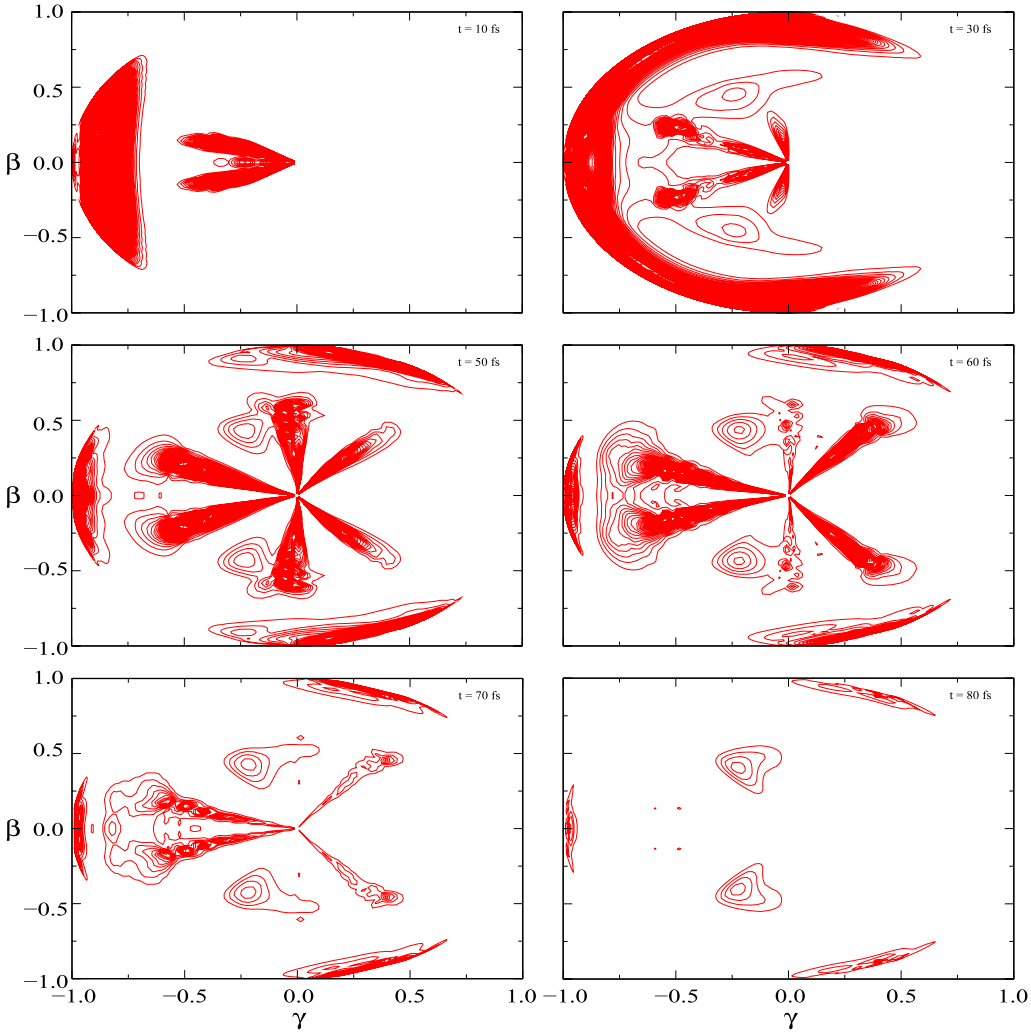

Fig. 5. Same as Fig. 3 as in Fig. 4 for $J = 20$.

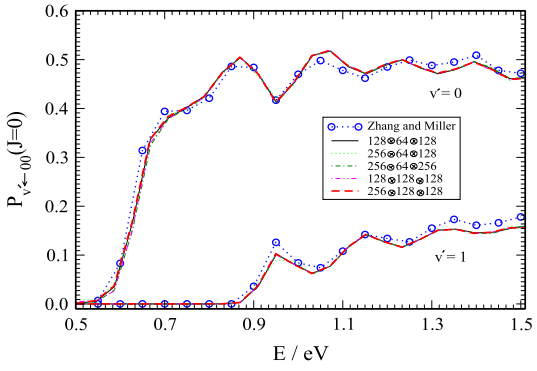

Fig. 6a. Vibrationally resolved reaction probabilities for $J = 0$ with the H_2 molecule initially on the $v = 0, j = 0$ state. All calculations are performed on SLTH PES, where convergence of reaction probabilities are shown as function of basis set: black (128 ⊗ 64 ⊗ 128), bright green (256 ⊗ 64 ⊗ 128), deep green (256 ⊗ 64 ⊗ 256), magenta (128 ⊗ 128 ⊗ 128) and red (256 ⊗ 128 ⊗ 128), whereas the blue circles depict Zhang and Miller's results [J. Chem. Phys. **91**, 1528 (1989)]. (For interpretation of the references to colour in this figure legend, the reader is referred to the web version of this article.)

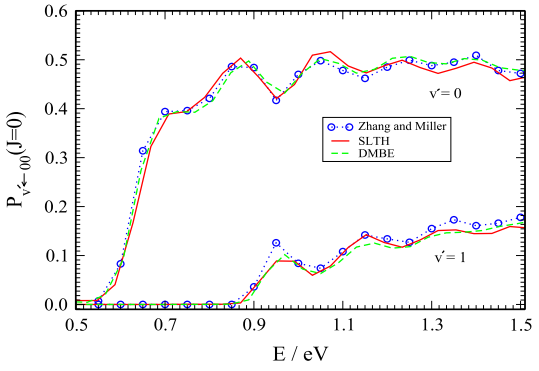

Fig. 6b. Vibrationally resolved reaction probabilities for $J = 0$ with the H_2 molecule initially in the $v = 0, j = 0$ state. Red line: SLTH (256⊗64⊗128); green line: DMBE (256 ⊗ 64 ⊗ 128); circle (blue) symbols: Zhang and Miller's results [J. Chem. Phys. **91**, 1528 (1989)]. (For interpretation of the references to colour in this figure legend, the reader is referred to the web version of this article.)

function of total angular momentum of the system (J) at various initial kinetic energies of the incoming atom, D. The agreement with the results of Zhang and Miller looks close enough for $v' = 0$ case (see Fig. 10), but disagreements are observed for $v' = 1$ (see Fig. 11).

5. Summary

We have implemented a time-dependent 3D ($J = 0$) as well as coupled 3D ($J \neq 0$) wave packet approach for any triatomic reactive system in hyperspherical coordinates so that all channels are even handedly treated. The method involves a grid representation for the hyperspherical coordinates (ρ, θ, ϕ), where the

Table 1
Data for the initialization, projection, absorbing potential discussed in the text. Run 1: $v = 0, j = 0, J = 0, 1, \ldots, 25$; Run 2: $v = 1, j = 0, J = 0$.

Grid size:			
N_ρ		256	
N_θ		64	
N_ϕ		128	
$(\rho_{\min}, \rho_{\max})$/Å		(0.85, 7.15)	
Molecular constants:			
D_e/eV		4.748	
r_e/Å		0.741	
β/Å^{-1}		1.950	
Translational wave packet:			
R_0/Å		3.50	
R_f/Å		1.68	
σ/Å		0.21	
k_0 (Å^{-1})	22.76 (Run 1)		15.12 (Run 2)
Initial state:			
E_{vj} (eV)	0.2706 (Run 1)		0.7864 (Run 2)
Propagation:			
Δt (10^{-16} s)		0.50	
Magnitude of the five last Lanczos vectors[a]		10^{-8}–10^{-7}	
Absorbing potential:			
$V_{\text{Im}}^{\max}$/eV		2.07	
α[b] (Å)		0.30–0.20	
Range of the absorbing potential (Å)		5.50–7.15	
Projection:			
R (Å)		2.75	
ρ range (Å)		2.83–3.99	
Vib. states		$v' = 0, \ldots, 2$	
Rot. states		$j' = 0, \ldots, 12$	

[a] The vectors are normalized, i.e., the total magnitude of all vectors is one.
[b] α is decreased linearly during the absorption of the wave packet.

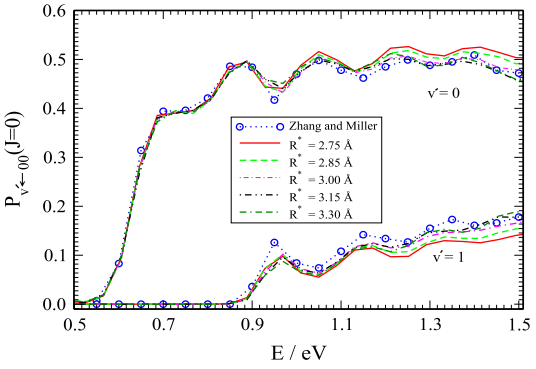

Fig. 6c. Vibrationally resolved reaction probabilities for $J = 0$ with the H_2 molecule initially in the $v = 0, j = 0$ state as a function R^* (asymptote projection distance). Red line: SLTH (256 ⊗ 64 ⊗ 128); green line: DMBE (256 ⊗ 64 ⊗ 128); circle (blue) symbols: Zhang and Miller's results [J. Chem. Phys. **91**, 1528 (1989)]. (For interpretation of the references to colour in this figure legend, the reader is referred to the web version of this article.)

rotation of the triatomic plane is quantized through a basis set expansion. By employing this approach, calculated reaction probabilities as a function of initial kinetic energy of the incoming atom (D) for the D + H_2 system agrees reasonably with Zhang and Miller's results [17] for $J = 0$ and $J \neq 0$ cases. Some disagreements at higher energies could conceivably be due to the following reasons: (i) single-energy dynamical calculation and projection over the entire energy range; (ii) time-dependent versus time-independent methodologies. Of course, we cannot exclude even if remotely, the possibility that it may also be due to the subroutine that has been utilized in the various calculations for the ground BO PES.

The present approach has two advantages: (a) the number of bases required for the quantization of the rotation of triatomic

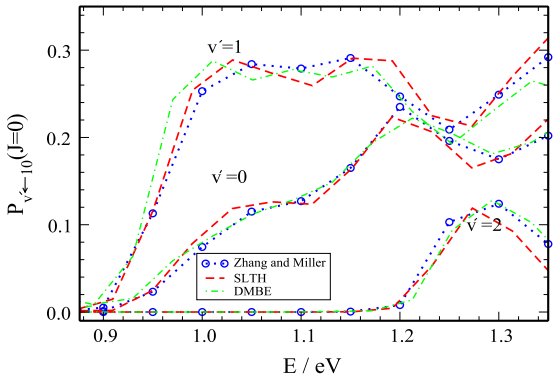

Fig. 7. Vibrationally resolved reaction probabilities for $J = 0$ with the H_2 molecule initially in the $v = 1, j = 0$ state. Square (red) symbols: present results using SLTH potential (256 ⊗ 64 ⊗ 128); circle (blue) symbols: Zhang and Miller's results [J. Chem. Phys. **91**, 1528 (1989)]. (For interpretation of the references to colour in this figure legend, the reader is referred to the web version of this article.)

plane are usually smaller than the number of grid points needed to represent the other internal DOF; (b) the algorithm can be quite efficiently parallelizable leading to the same computational (clock) time with increasing J except for the overhead due to the projection on various rovibrational states (v', j') for different orbital angular momentum, l'. Although the other time consuming part is the use of FFT for evaluating the kinetic energy operator, the vectorization of the grid through the implementation of parallel FFT algorithm reduces the computational time immensely. Since our principal aim is to extend the method to multi-surface problems, the present approach based on hyperspherical coordinates will be easy to implement almost without increasing the computational time.

Acknowledgments

SA acknowledges DST, India, through project no. SR/S1/PC-13/2008 for the research funding, and AJCV the financial support of FEDER through "Programa Operacional Factores de Competitividade—COMPETE" and national funds under the auspices of Fundação para a Ciência e a Tecnologia, Portugal. They also acknowledge Mr. Tapas Sahoo and Dr. Rahul Sharma for their help at various stages of computation.

Appendix A. Transformations between Jacobi and hyperspherical coordinates

Since we need to use Jacobi coordinates asymptotically to define the initial wave function of the triatomic system and wish to perform the dynamics in hyperspherical coordinates, it is necessary to establish the relations between these two sets of coordinates. Consider a space-fixed coordinate system (X', Y', Z') such that the three atoms A, B, C initially lie on the (X', Y') plane (see Fig. 1). If the diatom (B–C) and the incoming atom A coincide with the Y' and X' axis, respectively, the orientation of the **R** vector will be defined by the angles, $\Theta' = \pi/2$ and $\Phi' = 0$ (see Fig. 1) in the space-fixed coordinate system. On the other hand, the orientation of the **r** vector for the diatomic molecule will be specified by the angles, η and ξ in the body-fixed coordinate system.

In order to find the position vectors $\mathbf{r}'$ and $\mathbf{R}'$ at any point in the configuration space, we use the following relations:

$$\mathbf{r}' = \tilde{\mathbf{O}}\mathbf{r}, \tag{A.1}$$

$$\mathbf{R}' = \tilde{\mathbf{O}}\mathbf{R}, \tag{A.2}$$

where $\tilde{\mathbf{O}}$ specifies the rotation matrix defining the rotation of the triangle formed by the three atoms.

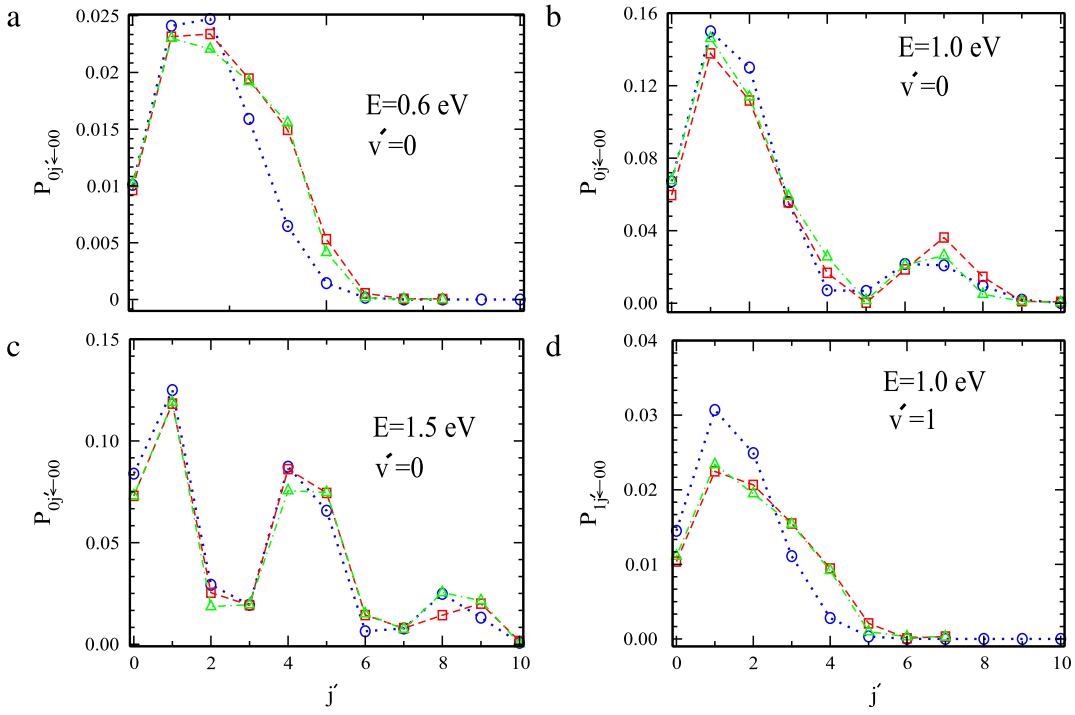

Fig. 8. Rotational distributions for $J = 0$ at 0.6 eV (a), 1.0 eV (b and d) and 1.5 eV (c). Square (red) symbols: SLTH (256⊗64⊗128); triangle up (green): DMBE (256⊗64⊗128); circle (blue) symbols: Zhang and Miller's results [J. Chem. Phys. **91**, 1528 (1989)]. (For interpretation of the references to colour in this figure legend, the reader is referred to the web version of this article.)

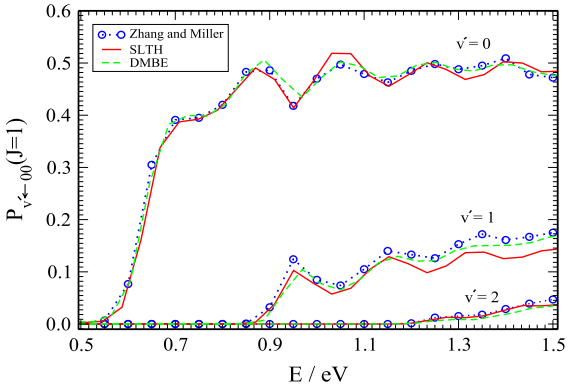

Fig. 9. Vibrationally resolved reaction probabilities for $J = 1$ with the H_2 molecule initially in the $v = 0$, $j = 0$ state. Red line: SLTH (256 ⊗ 64 ⊗ 128); green line: DMBE (256 ⊗ 64 ⊗ 128); circle (blue) symbols: Zhang and Miller's results [J. Chem. Phys. **91**, 1528 (1989)]. (For interpretation of the references to colour in this figure legend, the reader is referred to the web version of this article.)

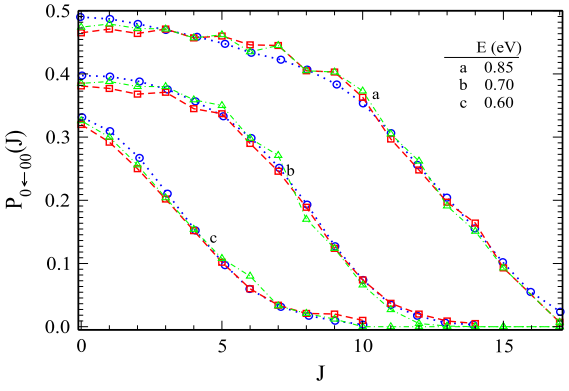

Fig. 10. Reaction probability D + H_2 ($v = 0$, $j = 0$) → HD($v' = 0$, all j') + H as a function of J, for several values of E(eV). Square (red) symbols: SLTH (256⊗64⊗128); triangle up (green): DMBE (256⊗64⊗128); circle (blue) symbols: Zhang and Miller's results [J. Chem. Phys. **91**, 1528 (1989)].

The definition of the hyperspherical coordinates in terms of the above mass-weighted Cartesian coordinates is introduced as

$$r_x = -\frac{\rho}{\sqrt{2}}\left(\cos\frac{\theta}{2} + \sin\frac{\theta}{2}\right)\cos\frac{\phi}{2}, \tag{A.3}$$

$$R_x = \frac{\rho}{\sqrt{2}}\left(\cos\frac{\theta}{2} + \sin\frac{\theta}{2}\right)\sin\frac{\phi}{2}, \tag{A.4}$$

$$r_y = \frac{\rho}{\sqrt{2}}\left(\cos\frac{\theta}{2} - \sin\frac{\theta}{2}\right)\sin\frac{\phi}{2}, \tag{A.5}$$

$$R_y = \frac{\rho}{\sqrt{2}}\left(\cos\frac{\theta}{2} - \sin\frac{\theta}{2}\right)\cos\frac{\phi}{2}, \tag{A.6}$$

$$r_z = R_z = 0, \tag{A.7}$$

which in turn lead to

$$r^2 = r_x^2 + r_y^2 = \frac{1}{2}\rho^2(1 + \sin\theta\cos\phi), \tag{A.8}$$

$$R^2 = R_x^2 + R_y^2 = \frac{1}{2}\rho^2(1 - \sin\theta\cos\phi), \tag{A.9}$$

$$r^2 + R^2 = \rho^2, \tag{A.10}$$

and

$$\mathbf{r}\cdot\mathbf{R} = r_xR_x + r_yR_y = -\frac{1}{2}\rho^2\sin\theta\sin\phi. \tag{A.11}$$

The angle between the **r** and **R** vectors is known as:

$$\cos\gamma' = \frac{\mathbf{r}\cdot\mathbf{R}}{rR} = \frac{-\sin\theta\sin\phi}{\sqrt{1 - \sin^2\theta\cos^2\phi}}, \tag{A.12}$$

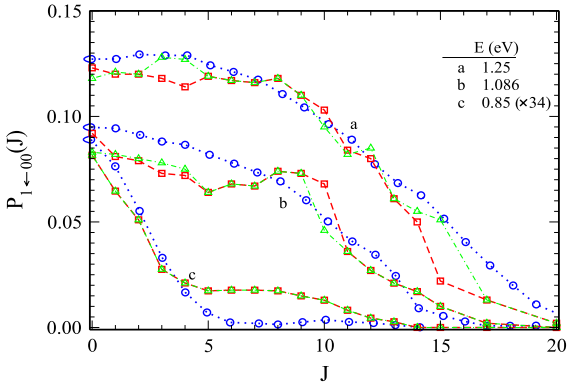

Fig. 11. Reaction probability D + H_2 ($v = 0, j = 0$) → HD($v' = 1$, all j') + H as a function of J, for several values of E(eV). Square (red) symbols: SLTH (256⊗64⊗128); triangle up (green): DMBE (256⊗64⊗128); circle (blue) symbols: Zhang and Miller's results [J. Chem. Phys. **91**, 1528 (1989)].

which, at $\rho \to \infty$, becomes identical to the diatomic orientation angle ($\gamma' = \eta$).

Since the AD states are expressed in term of spherical harmonics $Y_{j\mu}(\gamma', \xi)$ with γ', ξ defining the orientation of the diatomic molecule in a body-fixed coordinate system, the corresponding **R** vector along the Z-axis is given by

$$\mathbf{R} = (0, 0, R), \tag{A.13}$$

where the orientation of $\mathbf{R}'$ in a space-fixed coordinate system Θ' and Φ' also define the AD states and the angle Θ' can be evaluated as:

$$\mathbf{R}' = \tilde{\mathbf{O}}\mathbf{R} \tag{A.14}$$

$$\cos\Theta' = \frac{\mathbf{R}\cdot(0,0,1)}{|R'|} = \frac{R'_z}{R'}. \tag{A.15}$$

When we use the Euler's rotation matrix of the form given as in Eq. (A.16) (see Box I), in Eq. (A.14), we obtain

$$R'_z = \sin\beta\frac{\rho}{\sqrt{2}}\left(\cos\frac{\theta}{2}\sin\left(\gamma-\frac{\phi}{2}\right) - \sin\frac{\theta}{2}\sin\left(\gamma+\frac{\phi}{2}\right)\right). \tag{A.17}$$

While employing $R' = R$, the space-fixed orientation angle Θ' obtained from Eqs. (A.9) and (A.15) becomes

$$\cos\Theta' = \frac{\sin\beta\left(\cos\frac{\theta}{2}\sin\left(\gamma-\frac{\phi}{2}\right) - \sin\frac{\theta}{2}\sin\left(\gamma+\frac{\phi}{2}\right)\right)}{\sqrt{1-\sin\theta\cos\phi}}. \tag{A.18}$$

In the asymptotic limit, we substitute $\theta = \theta_0 = \pi/2$ to obtain:

$$\cos\Theta' = -\sin\beta\cos\gamma. \tag{A.19}$$

On the other hand, in order to determine ξ, we first rotate **r** to **r**′ (see Eq. (A.1)) and define a rotation of R' such that:

$$\mathbf{T}\mathbf{R}' = \begin{pmatrix}0\\0\\R'\end{pmatrix}. \tag{A.20}$$

With this rotated $\mathbf{R}'$ vector along the Z-axis in this body-fixed system, the orientation of $\mathbf{r}'$ in the same coordinate system becomes

$$r'' = \mathbf{T}\mathbf{r}' = \begin{pmatrix}r''_x\\r''_y\\r''_z\end{pmatrix} = \begin{pmatrix}r\ \sin\eta\ \cos\xi\\ r\ \sin\eta\ \sin\xi\\ r\ \cos\eta\end{pmatrix}, \tag{A.21}$$

with angles η and ξ.

When we substitute Eq. (A.1) in Eq. (A.21), we get

$$\begin{pmatrix}r''_x\\r''_y\\r''_z\end{pmatrix} = \mathbf{T}\tilde{\mathbf{O}}\begin{pmatrix}r_x\\r_y\\0\end{pmatrix}, \tag{A.22}$$

where the **T** matrix is given by

$$\mathbf{T} = \begin{pmatrix}\cos\Theta'\cos\Phi' & \cos\Theta'\sin\Phi' & -\sin\Theta'\\ -\sin\Phi' & \cos\Phi' & 0\\ \sin\Theta'\cos\Phi' & \sin\Theta'\sin\Phi' & \cos\Theta'\end{pmatrix}, \tag{A.23}$$

with Θ' and Φ' specifying the orientation of $\mathbf{R}'$ in the space-fixed coordinate system. Considering Eq. (A.22), we have

$$r''_z = \sum_{kl} T_{3k}\tilde{O}_{kl}r_l. \tag{A.24}$$

When we substitute Eq. (A.14) in Eq. (A.20), we get the following equation by using orthonormality condition of **T** matrix

$$T_{3j} = \frac{1}{R'}\sum_l \tilde{O}_{jl}R_l. \tag{A.25}$$

Inserting Eq. (A.25) and employing the orthonormality condition of $\tilde{\mathbf{O}}$ matrix, $\sum_k \tilde{O}_{km}\tilde{O}_{kl} = \delta_{ml}$ in Eq. (A.24), we obtain

$$\begin{aligned} r''_z &= \frac{1}{R'}\sum_{kl}\sum_m \tilde{O}_{km}\tilde{O}_{kl}R_m r_l \\ &= \frac{1}{R'}\sum_{lm}\left(\sum_k \tilde{O}_{km}\tilde{O}_{kl}\right)R_m r_l \\ &= \frac{1}{R'}(R_x r_x + R_y r_y). \end{aligned} \tag{A.26}$$

When we substitute Eq. (A.21) and Eqs. (A.3)–(A.6) in Eq. (A.26), we obtain

$$\cos\eta = \frac{-\sin\theta\sin\phi}{\sqrt{1-\sin^2\theta\cos^2\phi}}. \tag{A.27}$$

We can now use the same procedure to find $\sin\xi$ by considering r''_y,

$$r''_y = \sum_k T_{2k}\sum_l \tilde{O}_{kl}r_l = \sum_k T_{2k}\tilde{O}_{k1}r_x + \sum_k T_{2k}\tilde{O}_{k2}r_y \tag{A.28}$$

with ($r_z = 0$).

Introducing the following relations

$$\begin{aligned} T_{21} &= -\sin\Phi' = -\frac{R'_y}{R'\sin\Theta'} = -\frac{1}{R'\sin\Theta'}(\tilde{O}_{21}R_x + \tilde{O}_{22}R_y), \\ T_{22} &= \cos\Phi' = \frac{R'_x}{R'\sin\Theta'} = \frac{1}{R'\sin\Theta'}(\tilde{O}_{11}R_x + \tilde{O}_{12}R_y), \end{aligned} \tag{A.29}$$

leads to

$$r''_y = r\sin\eta\sin\xi = \frac{\cos\beta}{R'\sin\Theta'}\frac{\rho^2}{2}\cos\theta, \tag{A.30}$$

where we have used

$$\begin{aligned} &r_y R_x - r_x R_y = (\rho^2/2)\cos\theta, \\ &\tilde{O}_{11}\tilde{O}_{22} - \tilde{O}_{12}\tilde{O}_{21} = \cos\beta, \end{aligned} \tag{A.31}$$

with

$$rR' = \frac{1}{2}\rho^2\sqrt{1-\sin^2\theta\cos^2\phi} \tag{A.32}$$

and

$$\sin\eta = \frac{\cos\theta}{\sqrt{1-\sin^2\theta\cos^2\phi}}, \tag{A.33}$$

to finally obtain

$$\sin\xi = \cos\beta/\sin\Theta'. \tag{A.34}$$

$$\tilde{\mathbf{O}} = \begin{pmatrix} \cos\gamma\cos\alpha\cos\beta - \sin\alpha\sin\gamma & -\sin\gamma\cos\alpha\cos\beta - \sin\alpha\cos\gamma & \sin\beta\cos\alpha \\ \cos\gamma\cos\beta\sin\alpha + \sin\gamma\cos\alpha & \cos\alpha\cos\gamma - \sin\gamma\cos\beta\sin\alpha & \sin\beta\sin\alpha \\ -\cos\gamma\sin\beta & \sin\gamma\sin\beta & \cos\beta \end{pmatrix} \tag{A.16}$$

Box I.

Appendix B. Orthonormality of the initial wave packet

The normalization of the wave packet (see Eq. (14)) is defined as:

$$\sum \int d\rho\, d\theta\, d\phi |\Phi_k|^2 = 1. \tag{B.1}$$

If Eq. (23) is now considered, we may write:

$$\begin{aligned} \Phi_k^* \Phi_k = {} & 2\pi \sin\eta J(Rr\eta|\rho\theta\phi)(2l+1)\phi_{vj}^*(r)\phi_{vj}(r)\chi^* \\ & \times (R)\chi(R) \sum_{\mu}\sum_{\mu'} \begin{pmatrix} j & l & J \\ \mu & 0 & -\mu \end{pmatrix} \begin{pmatrix} j & l & J \\ \mu' & 0 & -\mu' \end{pmatrix} \\ & \times C_{j\mu}(\eta) C_{j\mu'}(\eta) A_{K\mu} A_{K\mu'}, \end{aligned} \tag{B.2}$$

where $J(Rr\eta|\rho\theta\phi)$ is a Jacobi factor and

$$J(Rr\eta|\rho\theta\phi)\, d\rho\, d\theta\, d\phi = dR\, dr\, d\eta, \tag{B.3}$$

$$\int dR\, \chi^*(R)\chi(R) = 1, \tag{B.4}$$

$$\int dr \phi_{vj}^*(r)\phi_{vj}(r) = 1, \tag{B.5}$$

leading to

$$\begin{aligned} & 2\pi \sum_K \int d\eta \sin\eta\, (2l+1) \sum_{\mu}\sum_{\mu'} \begin{pmatrix} j & l & J \\ \mu & 0 & -\mu \end{pmatrix} \\ & \times \begin{pmatrix} j & l & J \\ \mu' & 0 & -\mu' \end{pmatrix} C_{j\mu}(\eta) C_{j\mu'}(\eta) A_{K\mu} A_{K\mu'} = 1. \end{aligned} \tag{B.6}$$

Since

$$2\pi \int d\eta \sin\eta C_{j\mu}(\eta) C_{j\mu'}(\eta) = 1 \quad \text{only for } \mu = \mu' \tag{B.7}$$

and

$$(2l+1) \sum_{\mu} \begin{pmatrix} j & l & J \\ \mu & 0 & -\mu \end{pmatrix} \begin{pmatrix} j & l & J \\ \mu & 0 & -\mu \end{pmatrix} = 1, \tag{B.8}$$

the only possibility is

$$\sum_K A_{K\mu} A_{K\mu'} = \delta_{\mu\mu'}. \tag{B.9}$$

Appendix C. Sine transform

For a given ρ and ϕ, let us denote the amplitudes of the wave packet on the θ grid within the domain 0 to $\pi/2$ by

$$\chi(\theta_1), \chi(\theta_2), \ldots, \chi(\theta_{N-1}), \chi(\theta_N). \tag{C.1}$$

It is now important to note that while performing Fast Fourier transformation (FFT) on those amplitudes to evaluate the kinetic energy operator(s), the basis functions do not obey the boundary condition, *i.e.*, the corresponding cosine and sine functions do not vanish either at $\theta = 0$ or $\pi/2$, respectively. In order to resolve this problem, we double the grid with appropriate amplitudes as given below:

$$\begin{aligned} & \chi(\theta_1), \chi(\theta_2), \ldots, \chi(\theta_{N-1}), \chi(\theta_N), -\chi(\theta_N), -\chi(\theta_{N-1}), \ldots, \\ & -\chi(\theta_2), -\chi(\theta_1). \end{aligned} \tag{C.2}$$

The following scheme explores the necessity of doubling the grid in a symmetric manner with negative sign. Any one of the above discrete amplitudes ($\chi(\theta_l)s$) can be written in terms of Fourier coefficients:

$$\begin{aligned} \chi(\theta_k) &= \sum_{n=1}^{2N} C_n^k \exp(-i\kappa_n\theta_k), \quad \kappa_n = \frac{2\pi}{L};\ n \le N \\ &= \frac{2\pi}{L}(n-1-2N); \quad n > N \end{aligned} \tag{C.3}$$

where

$$C_m^l = \sum_{l=1}^{2N} \chi(\theta_l) \exp(i\kappa_m\theta_l)\Delta\theta. \tag{C.4}$$

If we now substitute the anti-symmetric form of the amplitudes (see Eq. (C.2)), Eq. (C.4) can be rewritten as:

$$\begin{aligned} C_m^l &= \sum_{l=1}^{N} 2i \sin(\kappa_m\theta_l)\Delta\theta; \quad m \le N \\ C_{m'}^l &= -\sum_{l=1}^{N} 2i \sin(\kappa_{2N-m+1}\theta_l)\Delta\theta; \quad m' > N. \end{aligned} \tag{C.5}$$

Therefore, we have

$$\begin{aligned} C_{2N}^l &= -C_1^l, \\ C_{2N-1}^l &= -C_2^l, \\ &\vdots \end{aligned} \tag{C.6}$$

and so on.

Accordingly, we have the following anti-symmetric string of Fourier coefficients for the lth amplitude, $\chi(\theta_l)$, of the wave packet:

$$C_1^l, C_2^l, \ldots, C_{N-1}^l, C_N^l, -C_N^l, -C_{N-1}^l, \ldots, -C_2^l, -C_1^l. \tag{C.7}$$

If we back substitute Eq. (C.7) in Eq. (C.3), we can rewrite the amplitudes, $\chi(\theta_1)$ and $\chi(\theta_{2N})$ as given below:

$$\begin{aligned} \chi(\theta_1) &= -2i \sum_{n=1}^{N} C_n^1 \sin(\kappa_n\theta_1), \\ \chi(\theta_{2N}) &= 2i \sum_{n=1}^{N} C_n^{2N} \sin(\kappa_n\theta_1). \end{aligned} \tag{C.8}$$

Thus, we find the following relationship:

$$\begin{aligned} \chi(\theta_{2N}) &= -\chi(\theta_1), \\ \chi(\theta_{2N-1}) &= -\chi(\theta_2), \\ &\vdots \end{aligned} \tag{C.9}$$

and so on.

which has been assumed in Eq. (C.2) for the required Sine transformation. Moreover, it is important to note that in this scheme, either the amplitudes (Eq. (C.8)) or the Fourier coefficients (Eq. (C.5)) are expressed in terms of sine functions.

Appendix D. Time energy Fourier transform

The relationship between the weight in k space of a given component of a Gaussian wave packet (see Eq. (28)) and its weight in energy space is derived via the free particle propagator [44]

$$K(R, t=0; R^*, t) = \left(\frac{\mu}{2\pi i\hbar t}\right)^{\frac{1}{2}} \exp\left[\frac{i\mu(R^*-R)^2}{2\hbar t}\right]. \tag{D.1}$$

The amplitude of the wave packet at a specified time, t, and point in space, R^*, can be expressed as

$$\chi(t, R^*) = \int_{-\infty}^{\infty} dR\, K(R, 0; R^*, t)\chi(t=0, R). \tag{D.2}$$

The Fourier transformation from time to energy space is now performed,

$$\begin{aligned} b(E; R^*) &= \frac{1}{\sqrt{2\pi}} \int_{-\infty}^{\infty} dt\, \chi(t, R^*) \exp(iEt/\hbar) \\ &= \frac{1}{\sqrt{2\pi}} Nc \int_{-\infty}^{\infty} dR \left[\int_{-\infty}^{\infty} dt\, t^{\gamma-1} \right. \\ &\quad \left. \times \exp\left(\frac{i\alpha}{2}\left(t - \frac{\beta^2}{t}\right)\right)\right] \exp[-ik_0 R - a(R-R_0)^2], \end{aligned} \tag{D.3}$$

where

$$c = \sqrt{\frac{\mu}{2\pi i\hbar}}, \tag{D.4}$$

$$\gamma = 1/2, \tag{D.5}$$

$$\alpha = \frac{2E}{\hbar} = \frac{\hbar k^2}{\mu}, \tag{D.6}$$

$$\beta = i\sqrt{\frac{\mu}{2E}}(R^* - R). \tag{D.7}$$

The integral in brackets can be solved analytically [45] giving

$$I = \sqrt{\frac{2\pi i}{\alpha}} \exp[-ik(R^* - R)]. \tag{D.8}$$

Substitution of this result together with the expressions for c and α into Eq. (D.3) yields

$$\begin{aligned} b(E; R^*) &= \frac{\mu}{\hbar k} \exp(-ikR^*) \frac{1}{\sqrt{2\pi}} N \int_{-\infty}^{\infty} dR \\ &\quad \times \exp[-ik_0 R - a(R-R_0)^2] \exp(ikR) \\ &= \frac{\mu}{\hbar k} \exp(-ikR^*) \frac{1}{\sqrt{2\pi}} \int_{-\infty}^{\infty} dR\, \chi(t=0, R) \\ &\quad \times \exp(ikR) = \frac{\mu}{\hbar k} \exp(-ikR^*) c_k. \end{aligned} \tag{D.9}$$

Thus, we have shown that

$$|c_E|^2 = \left(\frac{\mu}{\hbar k}\right)^2 |c_k|^2. \tag{D.10}$$

References

[1] Y.T. Lee, Chem. Scr. 27 (1987) 215; Science 236 (1987) 793.
[2] D.A.V. Kliner, D.E. Adelman, R.N. Zare, J. Chem. Phys. 95 (1991) 1648; F. Fernandez-Alonso, B.D. Bean, R.N. Zare, J. Chem. Phys. 111 (1999) 2490.
[3] E. Wrede, L. Schnieder, J. Chem. Phys. 107 (1997) 786; E. Wrede, L. Schnieder, K.H. Welge, F.J. Aoiz, L. Banares, J.F. Castillo, B. Martinez-Haya, V.J. Herrero, J. Chem. Phys. 110 (1999) 9971.
[4] P. Casvecchia, Rep. Progr. Phys. 63 (2000) 355.
[5] M. Baer, M. Faubel, B. Martinez-Haya, L.Y. Rusin, U. Tappe, J.P. Toennies, J. Chem. Phys. 110 (1999) 10231.
[6] S.A. Nizkorodov, W.W. Harper, W.B. Chapman, B.W. Blackman, D.J. Nesbitt, J. Chem. Phys. 111 (1999) 8404.
[7] G. Dharmasena, K. Copeland, J.H. Young, R.A. Lasell, T.R. Phillips, G.A. Parker, M. Keil, J. Phys. Chem. A 101 (1997) 6429.
[8] X. Liu, J.J. Lin, S.A. Harich, G.C. Schatz, X. Yang, Science 289 (2000) 1536.
[9] B. Liu, J. Chem. Phys. 80 (1984) 581; P. Siegbahn, B. Liu, J. Chem. Phys. 68 (1978) 2457; D.G. Truhlar, C.J. Horowitz, J. Chem. Phys. 68 (1978) 2466.
[10] A.J.C. Varandas, F.B. Brown, C.A. Mead, D.G. Truhlar, N.C. Blasis, J. Chem. Phys. 86 (1987) 6258.
[11] M. Cernei, Alexander Alijah, A.J.C. Varandas, J. Chem. Phys. 118 (2003) 2637.
[12] D.J. Diestler, V. McKoy, J. Chem. Phys. 48 (1968) 2951; E.M. Mortenson, K.S. Pitzer, J. Chem. Phys. 48 (1968) 4029; D.J. Truhlar, A. Kuppermann, J. Chem. Phys. 52 (1970) 3841; G.C. Schatz, J. Bowman, A. Kuppermann, J. Chem. Phys. 58 (1973) 4023; G.C. Schatz, J. Bowman, A. Kuppermann, J. Chem. Phys. 63 (1975) 674; C.C. Rankin, J.C. Light, J. Chem. Phys. 51 (1969) 1701; G. Miller, J.C. Light, J. Chem. Phys. 54 (1971) 1635; M. Baer, D.J. Kouri, Chem. Phys. Lett. 24 (1974) 37; M. Baer, J. Chem. Phys. 60 (1974) 1067; A. Persky, M. Baer, J. Chem. Phys. 60 (1974) 133; M. Baer, U. Halavee, A. Persky, J. Chem. Phys. 61 (1974) 5122; P.B. Middleton, R.E. Wyatt, J. Chem. Phys. 56 (1972) 2720; E.A. McCollough, R.E. Wyatt, J. Chem. Phys. 54 (1971) 3578.
[13] M. Baer, D.J. Kouri, Chem. Phys. Lett. 11 (1971) 238; J. Chem. Phys. 56 (1972) 1758; J. Chem. Phys. 57 (1972) 3991.
[14] R.P. Saxon, J.C. Light, J. Chem. Phys. 56 (1972) 3835; A. Altenberger-Siczek, J.C. Light, J. Chem. Phys. 61 (1974) 4373.
[15] A.B. Elkowitz, R.E. Wyatt, J. Chem. Phys. 62 (1975) 2504; A. Harms, R.E. Wyatt, J. Chem. Phys. 62 (1975) 3162.
[16] G. Wolken, M. Karplus, J. Chem. Phys. 60 (1974) 351.
[17] J.Z.H. Zhang, S.-I. Chu, W.H. Miller, J. Chem. Phys. 88 (1988) 6233; J.Z.H. Zhang, W.H. Miller, Chem. Phys. Lett. 140 (1987) 329; J. Chem. Phys. 88 (1988) 4549; Chem. Phys. Lett. 153 (1988) 465; J. Chem. Phys. 91 (1989) 1528.
[18] A. Kuppermann, G.C. Schatz, M. Baer, J. Chem. Phys. 65 (1976) 4596; A. Kuppermann, G.C. Schatz, M. Baer, J. Chem. Phys. 61 (1974) 4362.
[19] A. Kuppermann, G.C. Schatz, J. Chem. Phys. 62 (1975) 2502; G.C. Schatz, A. Kuppermann, Phys. Rev. Lett. 35 (1975) 1266; G.C. Schatz, A. Kuppermann, J. Chem. Phys. 65 (1976) 4642.
[20] F. Webster, J.C. Light, J. Chem. Phys. 85 (1986) 4744; F. Webster, J.C. Light, J. Chem. Phys. 90 (1989) 265.
[21] A. Kuppermann, P.G. Hipes, J. Chem. Phys. 84 (1986) 5962; P.G. Hipes, A. Kuppermann, Chem. Phys. Lett. 133 (1987) 1; G.A. Parker, R.T. Pack, B.J. Archer, R.B. Walker, Chem. Phys. Lett. 137 (1987) 564; R.T. Pack, G.A. Parker, J. Chem. Phys. 87 (1987) 3888; G.C. Schatz, Chem. Phys. Lett. 180 (1988) 92; G.C. Schatz, Chem. Phys. Lett. 151 (1988) 409; M. Mishra, J. Linderberg, Y. Ohrn, Chem. Phys. Lett. 111 (1984) 439; J.M. Launay, B. Lepetit, Chem. Phys. Lett. 144 (1988) 346.
[22] K. Hang, D.W. Schwenke, Y. Shima, D.G. Truhlar, J.Z.H. Zhang, D.K. Kouri, J. Phys. Chem. 90 (1986) 6757; K. Hang, D.W. Schwenke, D.G. Truhlar, Y. Zhang, J.Z.H. Zhang, D.J. Kouri, J. Phys. Chem. 87 (1987) 1892; D.W. Schwenke, K. Haug, D.G. Truhlar, Y. Sun, J.Z.H. Zhang, D.J. Kouri, J. Phys. Chem. 91 (1987) 6080; J.Z.H. Zhang, D.J. Kouri, K. Hang, D.W. Schwenke, Y. Shima, D.G. Truhlar, J. Phys. Chem. 88 (1988) 2492; M. Mladenovic, M. Zhao, D.G. Truhlar, D.W. Schwenke, Y. Sun, D.G. Kouri, Chem. Phys. Lett. 146 (1988) 358; Y.C. Zhang, J.Z.H. Zhang, D.J. Kouri, K. Hang, D.W. Schwenke, D.G. Truhlar, Phys. Rev. Lett. 60 (1988) 2367; M. Mladenovic, M. Zhao, D.G. Truhlar, D.W. Schwenke, Y. Sun, D.J. Kouri, J. Phys. Chem. 92 (1988) 7035.
[23] M. Baer, D.J. Kouri, Phys. Rev. A 4 (1971) 1924.
[24] B.K. Kendrick, L. Jayasinghe, S. Moser, M. Auzinsh, N. Shafer-ray, Phys. Rev. Lett. 84 (2000) 4325; B.K. Kendrick, J. Chem. Phys. 112 (2000) 5679.
[25] M. Baer, M. Faubel, B. Martinez-Haya, L.Y. Rusin, U. Tappe, J.P. Toennies, J. Chem. Phys. 108 (1998) 9694; M. Baer, M. Faubel, B. Martinez-Haya, L.Y. Rusin, U. Tappe, J.P. Toennies, J. Chem. Phys. 110 (1999) 10231.
[26] D. Sokolovski, J.F. Castillo, Phys. Chem. Chem. Phys. 2 (2000) 507; A.J. Dobbyn, P. McCabe, J.N.L. Connor, J.F. Castillo, Phys. Chem. Chem. Phys. 1 (1999) 1115; J.F. Castillo, D.E. Manolopoulos, K. Stark, H.-J. Werner, J. Chem. Phys. 104 (1996) 6531.
[27] Y.-S.M. Wu, S.A. Cuccaro, P.G. Hipes, A. Kuppermann, Chem. Phys. Lett. 168 (1990) 429; J.D. Kress, R.T. Pack, G.A. Parker, Chem. Phys. Lett. 170 (1990) 306; J.M. Launay, M. Le Dourneuf, Chem. Phys. Lett. 169 (1990) 473;

Leptit, A. Kuppermann, Chem. Phys. Lett. 166 (1990) 581;
Y.-S.M. Wu, B. Leptit, A. Kuppermann, Chem. Phys. Lett. 186 (1991) 319;
J.F. Castillo, D.E. Manolopoulos, Faraday Discuss. Chem. Soc. 110 (1998) 119;
M.P. de Miranda, D.C. Clary, J.F. Castillo, D.E. Manolopoulos, J. Chem. Phys. 108 (1998) 119;
D. Skouteris, D.E. Manolopoulos, W. Bian, W.-J. Werner, L.-H. Lai, K. Liu, Science 286 (1999) 1713;
A. Lagana, A. Bolloni, S. Crocchianti, G.A. Parker, Chem. Phys. Lett. 324 (2000) 466;
P. Honvault, J.-M. Launay, J. Chem. Phys. 111 (1999) 6665;
F. Huarte-Larranaga, X. Gimenez, J.M. Lucas, A. Aguilar, J.-M. Launay, Phys. Chem. Chem. Phys. 1 (1999) 1125.
[28] D. Neuhauser, M. Baer, R.S. Judson, D.J. Kouri, J. Chem. Phys. 90 (1989) 5882;
D. Neuhauser, M. Baer, J. Chem. Phys. 91 (1989) 4651;
D. Neuhauser, M. Baer, R.S. Judson, D.J. Kouri, Chem. Phys. Lett. 91 (1990) 372.
[29] E.M. Goldfield, S.K. Gray, Comput. Phys. Comm. 98 (1996) 1.
[30] D.H. Zhang, S.-Y. Lee, M. Baer, J. Chem. Phys. 112 (2000) 9802.
[31] A.J.H.M. Meijer, E.M. Goldfield, J. Chem. Phys. 110 (1999) 870.
[32] R.S. Judson, D.J. Kouri, D. Neuhauser, M. Baer, Phys. Rev. A 42 (1990) 351;
F. Gogtas, G.G. Balint-Kurti, A.R. Offer, J. Chem. Phys. 104 (1996) 7927.
[33] W. Zhu, T. Peng, J.Z.H. Zhang, J. Chem. Phys. 106 (1997) 1742;
T. Peng, J.Z.H. Zhang, J. Chem. Phys. 105 (1996) 6072;
D.J. Kouri, D.K. Hoffman, T. Peng, J.Z.H. Zhang, Chem. Phys. Lett. 262 (1996) 519.
[34] S.C. Althorpe, D.J. Kouri, D.K. Hoffmann, J. Phys. Chem. A 102 (1998) 9494; J. Chem. Phys. 107 (1997) 7816; J. Chem. Phys. 106 (1997) 7629; Chem. Phys. Lett. 275 (1997) 173.
[35] T. Peng, W. Zhu, D. Wang, J.Z.H. Zhang, Faraday Discuss. 110 (1998) 159.
[36] S.C. Althorpe, Faraday Discuss. 110 (1998) 238; J. Chem. Phys. 114 (2001) 1601; J. Chem. Phys. 117 (2002) 4623; Chem. Phys. Lett. 370 (2003) 443;
J.C. Juanes-Marcos, S.C. Althorpe, Chem. Phys. Lett. 381 (2003) 743;
S.C. Althorpe, J. Phys. Chem. 107 (2003) 7152; J. Chem. Phys. 121 (2004) 1175;
Phys. Rev. A 69 (2004) 042702;
J.C. Juanes-Marcos, A.J.C. Varandas, S.C. Althorpe, J. Chem. Phys. 128 (2008) 211101.
[37] Stephen K. Gray, G.G. Balint-Kurti, J. Chem. Phys. 108 (1998) 950.
[38] G.D. Billing, N. Markovic, J. Chem. Phys. 99 (1993) 2674;
N. Markovic, G.D. Billing, J. Chem. Phys. 100 (1994) 1085.
[39] R.F. Lu, T.S. Chu, Y. Zhang, K.L. Han, A.J.C. Varandas, J.Z.H. Zhang, J. Chem. Phys. 125 (2006) 133108.
[40] S. Mahapatra, H. Köppel, L.S. Cederbaum, J. Chem. Phys. 105 (2001) 2321.
[41] A.M. Arthurs, A. Dalgarno, Proc. R. Soc. Lond. Ser. A 256 (1960) 540.
[42] B.R. Johnson, J. Chem. Phys. 79 (1983) 1916.
[43] A.J.C. Varandas, Chem. Phys. Lett. 138 (1987) 455.
[44] R.P. Feynmann, A.R. Hibbs, Quantum Mechanics and Path Integrals, McCraw-Hill, New York, 1965.
[45] I.S. Gradshteyn, I.M. Ryzhyk, Tables of Integrals, Series, and Products, Academic, New York, 1965.